Environmental Fluid Mechanics (2020) 20:415–432
https://doi.org/10.1007/s10652-019-09700-1

ORIGINAL ARTICLE

Hybrid modelling of low velocity zones in box culverts to assist upstream fish passage

Xinqian Leng[1] · Hubert Chanson[1]

Received: 15 January 2019 / Accepted: 14 June 2019 / Published online: 28 June 2019

Abstract
A culvert is a covered channel designed to pass water through an embankment. The recognition of the adverse ecological impacts of culverts on upstream fish passage is driving the development of new culvert design guidelines, with a focus on small-bodied fish species seeking low velocity zones to minimise energy expenditure. Herein a hybrid modelling technique was applied, combining physical modelling, one-dimensional theoretical calculation and three-dimensional computational fluid dynamics modelling. The results reveal fundamental turbulent processes that may affect small-body-mass fish navigability and provide new insights for the development of standard box culvert design guidelines. Systematic validations were performed to a wide range of initial conditions and smooth barrel geometries. A physical relationship was derived from numerical and experimental data of past and present studies, correlating the dimensionless flow area with a normalised local velocity V/V_{mean}.

Keywords Open channel flows · Low velocity zones · Box culvert barrel · Upstream fish passage · Hybrid modelling

1 Introduction

A culvert is a hydraulic structure designed to pass water as an open channel flow through an embankment, e.g. beneath a road [2, 14, 15] (Fig. 1). In terms of hydraulic engineering, the optimum design of a culvert yields the smallest barrel size compatible with an inlet control operation at design discharge [10, 11, 16]. The resulting design leads to large culvert barrel velocities for design and less-than-design flow conditions, with adverse impact on upstream fish passage [3, 28, 33]. The recognition of the ecological impacts of road crossings and culverts as fish barriers has driven the development of new culvert design guidelines, with a particular focus on small-body-mass fish in Australia [12, 13]. Fish behaviour during upstream passage is closely linked to the hydrodynamic environment and flow turbulence. The targeted fish species may react to the local turbulent features including secondary flow motions during upstream fish

✉ Xinqian Leng
xinqian.leng@uqconnect.edu.au

1 School of Civil Engineering, The University of Queensland, Brisbane, QLD 4072, Australia

Fig. 1 Standard box culverts. **a** Multicell box culvert outlet along Whitton Creek, below Kate St, Indooroopilly QLD, Australia in operation in 30 March 2017. **b** Pipe culvert outlet along Cubberla Creek beneath Greenford St, Chapel Hill QLD, Australia on 30 March 2017

passage, seeking low velocity zones (LVZs) to minimise its energy expenditure [31, 32]. Several types of boundary treatments, such as baffles and boundary roughening, may be installed along the culvert barrel invert to decrease the flow velocity and improve upstream fish passage [8, 9, 19, 29], but the additional flow resistance can reduce drastically the culvert discharge capacity for a given afflux: "the installation of baffles in a culvert drastically reduces its capacity" [20]; "the discharge capacity of the full-pipe nonpressurized flow weir baffled culvert produced was approximately 50 to 70% less than the smooth walled culvert for the range of [test]" [28].

In the present work, an integrated modelling technique was applied, by combining physical modelling, one-dimensional (1D) theoretical calculation and three-dimensional computational fluid dynamics modelling (3D CFD) of a standard box culvert barrel. Detailed CFD validation was undertaken against laboratory studies obtained under carefully controlled flow conditions. This study focuses on the upstream passage of small-bodied native species in Australia, with initial tests undertaken with juvenile silver perch (*Bidyanus*

bidyanus) and Duboulay's rainbowfish (*Melanotaenia duboulayi*) in a 12 m long 0.5 m wide culvert barrel channel [7, 9, 32].

2 Numerical CFD model: methodology and configuration

2.1 Methodology

In the current study, some hybrid modelling was conducted, combining physical experiments, one-dimensional theoretical calculations, and numerical CFD calculations. In practice, a culvert structure can range from a few metres to 30 m in length, with a single cell being typically 0.5 m to 3 m in width and height. As a result, modelling large culvert cells using physical experiments in laboratory may be a challenge. Numerical CFD modelling was used mainly herein, coupled with the 1D theoretical calculation (backwater calculations) to pre-determine the free-surface level at the numerical inlet and outlet.

The CFD model solves the Navier–Stokes equations of fluid motion using numerical method. The Navier–Stokes equations in its incompressible two-phase flow form can be written as:

$$\nabla \cdot \vec{u} = 0 \tag{1}$$

$$\rho\left(\frac{\partial \vec{u}}{\partial t} + \left(\vec{u} \cdot \nabla\right)\vec{u}\right) = \rho\vec{g} - \nabla p + \nabla \cdot \left[\mu\left(\nabla\vec{u} + \nabla^{T}\vec{u}\right)\right] \tag{2}$$

where $\vec{u}$ is the velocity vector, p is the pressure, t is time, $\vec{g}$ is the gravity vector, ρ is the fluid density and μ is the fluid viscosity.

ANSYS^{TM} Fluent version 18.0 was used to conduct the CFD modelling. A standard k–ε model was used to solve the flow turbulence. For smooth turbulent flow through simplistic geometries, like a smooth box culvert barrel, the flow physics is mostly dominated by boundary shear on the bottom and sidewall boundaries. A simplistic turbulence model such as a k–ε model is sufficient to resolve the velocity field, with a relatively low computational cost. The simplified Reynolds Averaged Navier–Stokes equations are solved as [1]:

$$\frac{\partial \rho}{\partial t} + \frac{\partial}{\partial x_j}\left(\rho u_j\right) = 0 \tag{3}$$

$$\frac{\partial \rho\, u_i}{\partial t} + \frac{\partial}{\partial x_j}\left(\rho\, u_i u_j\right) = -\frac{\partial p'}{\partial x_i} + \frac{\partial}{\partial x_j}\left[\mu_{eff}\left(\frac{\partial u_j}{\partial x_j} + \frac{\partial u_j}{\partial x_i}\right)\right] + S_M \tag{4}$$

where S_M is the sum of body forces, μ_{eff} is the effective viscosity representing flow turbulence, and p' is the modified pressure, the subscriptions i and j represent properties in the i and j directions. Based on the "eddy viscosity" concept first proposed by Boussinesq [5], the effective viscosity may be calculated as:

$$\mu_{eff} = \mu + \mu_t \tag{5}$$

where μ and μ_t are respectively the fluid viscosity and eddy (turbulent) viscosity [1].

The standard k–ε model used two transport equations to describe the turbulent viscosity. The two equations are for the turbulent kinetic energy k and dissipation ε respectively [21]:

$$\frac{\partial}{\partial t}(\rho k) + \frac{\partial}{\partial x_i}(\rho k u_i) = \frac{\partial}{\partial x_j}\left[\left(\mu + \frac{\mu_t}{\sigma_k}\right)\frac{\partial k}{\partial x_j}\right] + G_k + G_b - \rho\varepsilon - Y_M + S_K \tag{6}$$

$$\frac{\partial}{\partial t}(\rho \varepsilon) + \frac{\partial}{\partial x_i}(\rho \varepsilon u_i) = \frac{\partial}{\partial x_j}\left[\left(\mu + \frac{\mu_t}{\sigma_\varepsilon}\right)\frac{\partial \varepsilon}{\partial x_j}\right] + C_{1\varepsilon}\frac{\varepsilon}{k}\left(G_k + C_{3\varepsilon}G_b\right) - C_{2\varepsilon}\rho\frac{\varepsilon^2}{k} + S_\varepsilon \tag{7}$$

where G_k represents the generation of turbulent kinetic energy due to the mean velocity gradient, G_b is the generation of turbulent kinetic energy due to buoyancy, Y_M represents the contribution of the fluctuating dilatation in compressible turbulence to the overall dissipation rate. $C_{1\varepsilon}$, $C_{2\varepsilon}$ and $C_{3\varepsilon}$ are constants, σ_k and σ_ε are the turbulent Prandtl numbers for k and ε respectively, S_k and S_ε are user-defined source terms. The turbulent viscosity μ_t is computed by combining k and ε as:

$$\mu_t = \rho C_\mu \frac{k^2}{\varepsilon} \tag{8}$$

By default, ANSYS Fluent used the following values for constants: $C_{1\varepsilon}, = 1.44$, $C_{2\varepsilon} = 1.92$, $C_\mu = 0.09$, $\sigma_k = 1.0$, $\sigma_\varepsilon = 1.3$ [1].

The two-phase flow interface in the culvert barrel was tracked by a volume of fluid (VOF) method [17]. In VOF, a colour function C is introduced, defined as 0 in one phase and 1 in the other. Herein, the primary phase was selected to be air (the lighter medium) and secondary phase water. The function C is characterised by an advection equation:

$$\frac{\partial C}{\partial t} + \vec{u}\cdot\nabla C = 0 \tag{9}$$

Fluid properties such as density and viscosity are then calculated based on respective fractions of local colour function.

The near-wall areas of the flow were treated by a built-in standard wall function in ANSYS Fluent the wall function was based on the work of Launder and Spalding [21], and is used widely in industrial flows. The log-law was applied for near-wall regions to calculate the dimensionless velocity u^* by:

$$u^* = \frac{1}{\kappa}\ln(E y^*) \tag{10}$$

where

$$u^* \equiv \frac{u_p C_\mu^{1/4} k_p^{1/2}}{\tau_w/\rho} \tag{11}$$

and:

$$y^* \equiv \frac{\rho C_\mu^{1/4} k_p^{1/2} y_P}{\mu} \tag{12}$$

and κ is the von Karman constant: $\kappa = 0.4187$, E is the empirical constant: $E = 9.793$, U_p is the mean velocity of the fluid at the wall-adjacent grid centroid P, k_p is the turbulence kinetic energy at the wall-adjacent gird centroid P, y_p is the distance from the centroid of the wall-adjacent grid to the wall, and μ is the dynamic viscosity of the fluid [1]. The log law for mean velocity is only valid for $30 < y^* < 300$. Herein, ANSYS Fluent employs the log law when $y^* > 11.225$. When the mesh yields $y^* < 11.225$ at the wall-adjacent grids, ANSYS Fluent applies the laminar stress–strain relationship:

$$u^* = y^* \tag{13}$$

When dealing with rough pipes and channels, the law-of-wall is modified to include a roughness effect as [1]:

$$u^* = \frac{1}{\kappa} \ln (E\, y^*) - \Delta B \tag{14}$$

ΔB is well-correlated with the non-dimensional roughness height K_s^+ calculated as:

$$K_s + = \frac{\rho k_s C_\mu^{1/4} k_p^{1/2}}{\mu} \tag{15}$$

where k_s is the equivalent roughness height. In ANSYS Fluent, three distinct roughness regimes are employed. For hydro-dynamically smooth regime ($K_s^+ \le 2.25$), $\Delta B = 0$. For a transitional regime ($2.25 \le K_s^+ \le 90$):

$$\Delta B = \frac{1}{\kappa} \ln \left[\frac{K_s^+ - 2.25}{87.75} + C_s K_s^+ \right] \times \sin \left\{ 0.4258 \left(\ln K_s^+ - 0.811 \right) \right\} \tag{16}$$

where C_s is a roughness constant (in this case $C_s = 0.5$ representing uniform roughness). In the fully rough regime ($K_s^+ \ge 90$):

$$\Delta B = \frac{1}{\kappa} \ln \left[1 + C_s K_s^+ \right] \tag{17}$$

Present study only focuses on smooth transitional turbulent flow, due to the scope of the study being box culvert with smooth concrete walls.

2.2 CFD model configuration

The numerical domain representing a single box culvert barrel is illustrated in Fig. 2. Two barrel lengths were modelled, i.e. L = 8 m and 12 m. The width B_{cell} and height D_{cell} of the numerical domain were prescribed and the values are detailed in Table 1. The inlet plane, marked by yellow and blue in Fig. 2, was split into two velocity inlets, one for water (coded yellow) and one for air (coded blue). The outlet plane, coded green in Fig. 2, was a single outlet for both phases, and set to be a pressure outlet. A free-surface level was required to set up the outlet for open channel flow, and this outlet depth d_{out} was prescribed according to the tailwater level for the modelled case. In general, $d_{out} \approx d_{tw}$, where d_{tw} was the tailwater depth in the floodplain downstream of the culvert barrel. The boundary conditions are summarised in Table 2.

The numerical CFD modelling consisted of two stages: (1) transient flow simulation in a 3D culvert channel with coarse mesh; the coarse mesh consisted of uniform squares with 0.05–0.1 m grid size throughout the numerical domain; and (2) transient flow simulation in

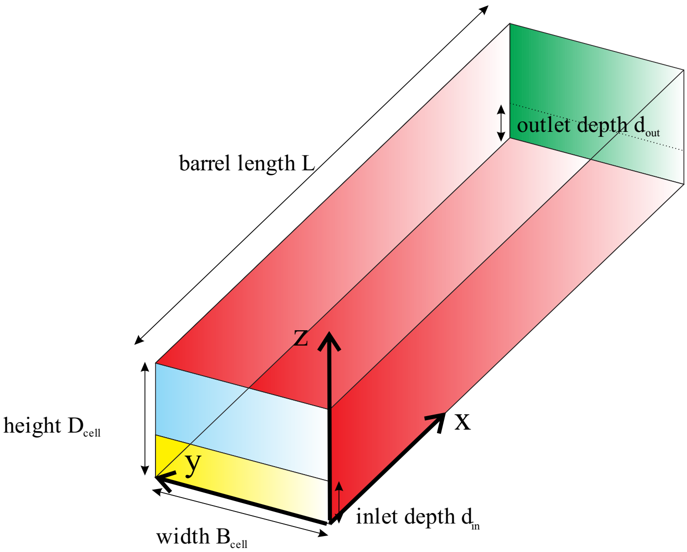

Fig. 2 Three-dimensional (3D) sketch of numerical domain with colour-coded boundaries; detailed boundary conditions listed in Table 2

a 3D culvert channel with refined mesh; the mesh was refined into non-uniform gradually varied squares using a bias function:

$$\Delta = \sum_{0}^{i} \Delta_1 \times r^i \tag{18}$$

where Δ is the size of the meshed edge, Δ_1 is the size of the first element calculated using a bias factor bf, r is the growth rate, $i = 1, 2, 3, \ldots, n-1$ with n being the number of divisions in grid on the meshed edge. The relationship between growth factor r, bias factor bf and number of division n is:

$$bf = r^{n-1} \tag{19}$$

Biased mesh with refinement near the walls and sidewalls were essential to simulate realistic flow patterns near the boundaries. A bias factor of 20–30 was typically used for all cases, resulting in a growth factor r = 1.1–1.2. After refinement, the smallest grid size in the vertical y and transverse z directions was between 0.001 and 0.005 m, depending on the size of the culvert barrel. Due to the computational cost and limit in time, large culvert structures were meshed with a slightly coarser grid, compared to small culvert structures. With full-scale large culvert structures, a range of mesh sizes were used, the coarsest mesh being 50 mm (vertical) by 50 mm (transverse) and 50 mm longitudinal, uniformly spaced, for a 2.4 m × 2.4 m × 8 m domain. Such dimensions were small compared to the boundary layer thickness and secondary current structures in the bottom corners of large culvert structures. The mesh in the stream-wise x-direction was uniformly partitioned with a grid size of 0.05 m to 0.1 m for all cases.

All models were solved using a k–ε method for turbulence. The transient formulation was solved implicitly with a second order upwind scheme for momentum, first order upwind scheme for turbulent kinetic energy and turbulent dissipation rate. The convergence

Table 1 Numerical CFD modelling of culvert barrel flows: detailed flow conditions

Case	Design flow conditions									10% design flow conditions						
	Q_{des} (m^3/s)	L (m)	S_o	d_{tw} (m)	afflux (m)	N_{cell}	B_{cell} (m)	D_{cell} (m)	Q_{cell} (m^3/s)	Q (m^3/s)	Q_{cell} (m^3/s)	d_{tw} (m)	q (m^2/s)	$(B/d)_{cell}$	V_{mean} (m/s)	Mesh grid number (longitudinal × vertical × transverse)
Gara River case	20	8	0	0.976	0.55	7	1.3	1	2.86	2	0.29	0.51	0.22	2.60	0.44	160×30×25
Exam paper case	4.8	14	0.0012	0.457	0.2	7	1	0.5	0.69	0.48	0.07	0.12	0.07	8.33	0.57	140×30×20
Laura River case	95	8	0.0015	2.195	0.45	10	2.4	2.4	9.50	9.5	0.95	0.51	0.40	4.71	0.80	160×48×48
Experiment 1		8	0				0.5	0.5			0.06	0.16	0.11	3.13	0.70	80×30×20
Experiment 2		12	0				0.5	0.5			0.03	0.10	0.05	5.00	0.52	240×30×25
Experiment 3		8	0.05				0.5	0.5			0.06	0.04	0.112	12.5	2.8	80×30×20
Experiment 4		8	0				0.5	0.5			0.11	0.30	0.22	1.67	0.75	80×30×20
Experiment 5		8	0				1	1			0.11	0.20	0.11	5.05	0.57	80×30×20
Experiment 6		19	0				0.7	0.5			0.10	0.10	0.14	4.24	0.87	380×30×20
Other 1	10	8	0.005	1	0.5	5	1	0.75	2.00	1	0.20	0.20	0.20	6.06	1.21	80×30×30

Table 2 Colour-coding of boundaries as shown in Fig. 2 and the boundary conditions

Colour	Boundary name	Boundary condition	Remarks
Blue	Air inlet	Velocity inlet	Inlet velocity $V_{in} = 0$ m/s
Yellow	Water inlet	Velocity inlet	Inlet velocity V_{in} calculated from inlet discharge
Red	Walls	Wall	Roughness $k_s = 0$–0.001 m (i.e. smooth concrete). Uniform roughness
Green	Outlet (air and water)	Pressure outlet	Free-surface level at outlet d_{out} set from tailwater level d_{tw} ($d_{out} = d_{tw}$ in general)

was ensured by reducing residuals of all parameters to 10^{-4} or less. All simulations were run until the monitored free-surface level at a location stopped varying or only showed very small fluctuations, and the conservation of mass was achieved between inlet and outlet at the end of the transient simulation. Typically, the physical time it took to reach this stage was 60–90 s. The computation time for a complete run was approximately 12–24 h on a HPC workstation (8 processors).

3 Detailed physical experiments

Detailed physical experiments were conducted based on a Froude similitude. A dimensional analysis yields the relationship between flow properties at a location (x, y, z) and the upstream flow conditions, channel geometry and fluid properties as:

$$d, \vec{V}, v', P, L_t, T_t, \ldots = F\left(x, y, z, B, k_s, S_o, d_1, V_1, v'_1, \rho, \mu, \sigma, g, \ldots\right) \tag{20}$$

where d is the flow depth, V is the local velocity, v′ is a local velocity fluctuation, P is the local pressure, L_t and T_t are local integral turbulent length and time scales, x, y and z are respectively the longitudinal, transverse and vertical coordinates, B is the internal barrel width, k_s is the equivalent sand roughness height of the barrel boundary, S_o is the invert slope ($S_o = \sin\theta$ with θ being the angle between bed and horizontal), d_1, V_1 and v′ are respectively the inflow depth, velocity and velocity fluctuation, ρ and μ are the water density and dynamic viscosity, σ is the surface tension, g is the gravity acceleration ($g = 9.8$ m/s^2). In Eq. (20), the 4th, 5th and 6th variables characterise the boundary conditions, the 7th, 8th and 9th terms define the inflow (initial) conditions, and the following terms are fluid and physical properties.

Systematic physical experiments were performed in a 12 m long, 0.5 m wide rectangular prismatic channel (Fig. 3a) [7, 9]. A number of discharges were tested, ranging from 0.026 to 0.0556 m^3/s. The channel bed was horizontal herein, i.e. $S_o = 0$. A horizontal slope was selected to reduce the number of independent variables in Eq. (20) and eliminate any gravity effects in relation to upstream fish passage. The flume was made of smooth PVC bed and glass walls. The waters were supplied by a constant head tank feeding a large intake basin (2.1 m long, 1.1 m wide, 1.1 m deep) leading to the test section through a series of flow straighteners, followed by convergent bottom and sidewalls. The channel outlet was a free overfall at $x = 12$ m, where x is the longitudinal distance from the upstream end of the test section, positive downstream. Stainless steel screens were installed at both upstream and downstream ends to ensure the safety of small fish. The flow rate was measured with an orifice meter that was designed based upon the

Fig. 3 Experimental facilities for studying fish passage under culverts. **a** 12 m long 0.5 m wide rectangular channel, with flow direction from background to foreground; experimental low conditions: $\theta = 0$, $Q = 0.0556\ m^3/s$, $d = 0.166$ m, $Re = 1.4 \times 10^5$, looking upstream [7]. **b** Single cell box culvert model at the University of Queensland (Australia) for $Q/Q_{des} = 1.2$ and different tailwater depth, (left) outlet operation for $d_{tw}/D = 1.1$, (right) submerged inlet operation for $d_{tw}/D = 1.1$

British Standards [6] and calibrated on site. The percentage of error was expected to be less than 2% on the discharge measurement. The water depths were measured using rail mounted pointer gauges with an accuracy of ±0.5 mm. Velocity measurements were conducted with a Prandtl-Pitot tube. The Pitot tube was a Dwyer® 166 Series Prandtl-Pitot tube with a 3.18 mm diameter tube made of corrosion resistant stainless steel, and featured a hemispherical total pressure tapping (Ø = 1.19 mm) at the tip and four equally spaced static pressure tappings (Ø = 0.51 mm) located 25.4 mm behind the tip. The translation of the Pitot-Prandtl probe in the vertical direction was controlled by a fine adjustment travelling mechanism connected to a Mitutoyo™ digimatic scale unit. The experimental flow conditions are detailed in Table 3A.

Table 3 Experimental flow conditions and numerical CFD models of the present study

(A)

Physical experiments [7]	Q (m^3/s)	L (m)	B (m)	S_o	d_1 (m)	V_1 (m/s)	Bed configuration
	0.0556	12	0.5	0	0.162	0.69	Smooth bed
	0.0261	12	0.5	0	0.096	0.54	Smooth bed

(B)

Present CFD study	Q (m^3/s)	L (m)	B_{cell} (m)	D_{cell} (m)	S_o	V_{in} (m)	d_{out} (m)	Mesh grid density	Δx_{min} (m)	Δy_{min} (m)	Δz_{min} (m)
	0.0556	8	0.5	0.5	0	0.56	0.160	55,398 nodes 50,480 elements	0.100	0.001	0.002
	0.0261	12	0.5	0.5	0	0.50	0.096	212,992 nodes 197,625 elements	0.002	0.002	0.003

Fish swimming behaviour and endurance were studied and analysed [8, 9, 32], with a focus on small-bodied native Australian fish: i.e., juvenile silver perch (*Bidyanus bidyamus*) and Duboulay's rainbowfish (*Melanotaenia duboulayi*). The physical observations showed that fish swim preferentially close to sidewalls, in regions of low velocity and high turbulence, as also reported by Blank [4] and Jensen [18] with other fish species. The presence of secondary currents is believed to impact on the fish swimming behaviour. Specifically, at regions where secondary currents are strong, i.e. in the two bottom corners of barrel, fish demonstrated better traversability. In the culvert channel, fish spent two-third of their time next to bottom corners, and nearly 90% of time next to sidewalls and bottom corners [7, 9, 32].

Additional physical measurements were conducted in a 1:10 single box culvert model at the hydraulic laboratory of the University of Queensland (Fig. 3b). The single box culvert model was located in a 1 m wide flume. Its barrel was 0.50 m long, 0.150 m wide and 0.105 m high. The culvert model gave physically-meaningful flow patterns, for different combination of discharges and tailwater conditions, and was used mostly for visual observations and free-surface measurements. Free-surface measurements were performed using a mounted point gauge at the culvert model inlet and outlet. Within the culvert barrel, transparent glass side walls enabled detailed observation of free-surface profile throughout the barrel length, when the barrel was not drowned. When drowned, point gauge was used again for depth measurements.

4 Hybrid model results and validation

4.1 Velocity field and low velocity zones

The CFD results were systematically compared to detailed laboratory measurements, with a focus on the water surface profile and the longitudinal velocity field, for less than design flow conditions. Table 3 presents the experimental flow conditions and the numerical model details, corresponding to these flow cases. Herein, the inflow discharge Q is the flow rate through the experimental channel, i.e. a single culvert barrel, L is the length of the experimental channel/numerical domain, B is the width of the experimental channel, B_{cell} and D_{cell} are the internal width and height of the numerical domain respectively, S_o is the barrel channel invert slope for both experimental and numerical studies, d_1 and V_1 are respectively the depth and velocity measured at 8 m downstream of the experimental channel inlet, V_{in} is the inlet velocity prescribed at the velocity inlet of the numerical model for water phase, d_{out} is the free-surface level prescribed at the pressure outlet of the numerical model, Δx_{min}, Δy_{min} and Δz_{min} are respectively the minimum mesh grid size in the longitudinal x, vertical y and transverse z directions. A grid convergence study was performed using a series of three successively refined mesh grids [30]. The effective grid refinement ratio was 2. Two parameters were used to assess the grid convergence, being the free-surface level (indicative of the mean velocity) and the area fraction of low velocity zone, i.e. the relative flow area for velocity less than 75% of the mean velocity. The final mesh grids used in the current study were chosen based on the study, so as to ensure the grid number was sufficient to yield a solution within the asymptotic range of convergence.

Figure 4 shows a comparison between the numerically simulated free-surface elevation and the experimental measurements. Typical comparison of velocity profiles are presented in Fig. 5, with centreline results shown on the right and data close to the sidewall on the left. The comparative results demonstrated a good agreement between the backwater calculation, CFD and experimental data in terms of free-surface elevation throughout the culvert channel (Fig. 4). A key point was the selection of a realistic tailwater depth d_{out}. The CFD model used a pressure outlet, which was very sensitive to the prescribed downstream free-surface level at the outlet. In the present study, experimentally-measured values were used at the outlet boundary to prescribe the tailwater depth, which was considered very important in reproducing the correct free-surface profile.

The vertical profiles of longitudinal velocity component at different transverse locations were compared to experimental results for validation purpose (Fig. 5). Both CFD and physical data showed the presence of low velocity zones (LVZs) along the wetted perimeter of the barrel cell: i.e., next to the sidewalls and the bottom corner, plus a thin region along the invert (Fig. 6). Overall the CFD data compared favourably to physical results for all transverse locations, with the locations near the sidewalls ($y = 0.08$ m and 0.42 m) being better modelled than the centre of the channel. The results showed an overall tendency of over-estimating longitudinal velocity magnitudes by the CFD numerical model, especially towards the centreline of the channel (Fig. 5 Right). The maximum longitudinal velocity was over-estimated by 10% using the CFD numerical model, compared to the experimental data for the flow $Q = 0.056$ m^3/s.

Overall the results showed the capacity of the CFD model to predict the three-dimensional flow field in a smooth culvert barrel at less than design discharges, for which upstream fish passage may be a design requirement. The systematic validation against physical data is uppermost critical to ascertain the performances of a numerical model, and can be sensitive to a range of inflow conditions, boundary parameters, and the grid mesh quality and size [22, 35].

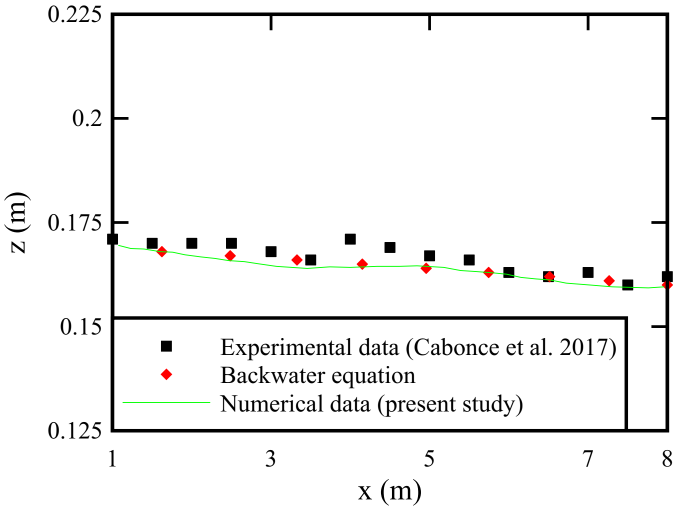

A $Q = 0.056\ m^3/s$

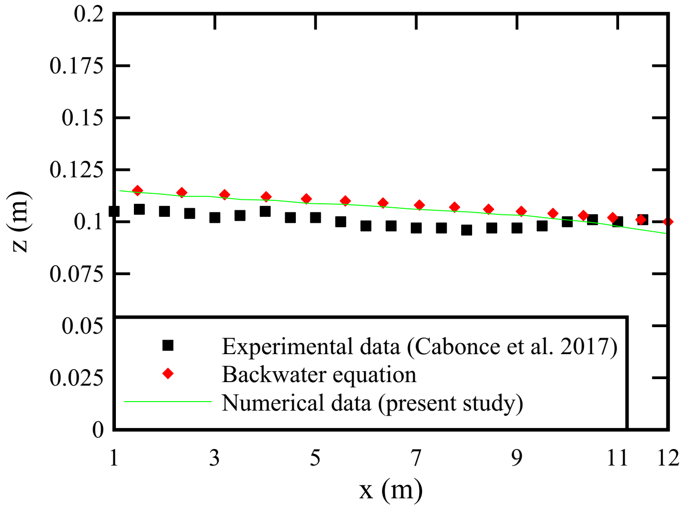

B $Q = 0.026\ m^3/s$

Fig. 4 Free-surface comparison between 1D backwater calculation, CFD and experimental results; experimental data from Cabonce et al. [7]; flow condition: **a** $Q=0.056\ m^3/s$, $f=0.0162$, **b** $Q=0.026\ m^3/s$, $f=0.0145$

4.2 Estimating the area fraction of low velocity zones

Because of the large number of relevant design parameters, e.g. design discharge Q_{des}, tailwater level d_{tw}, maximum afflux, box cell configuration etc., and the case specific

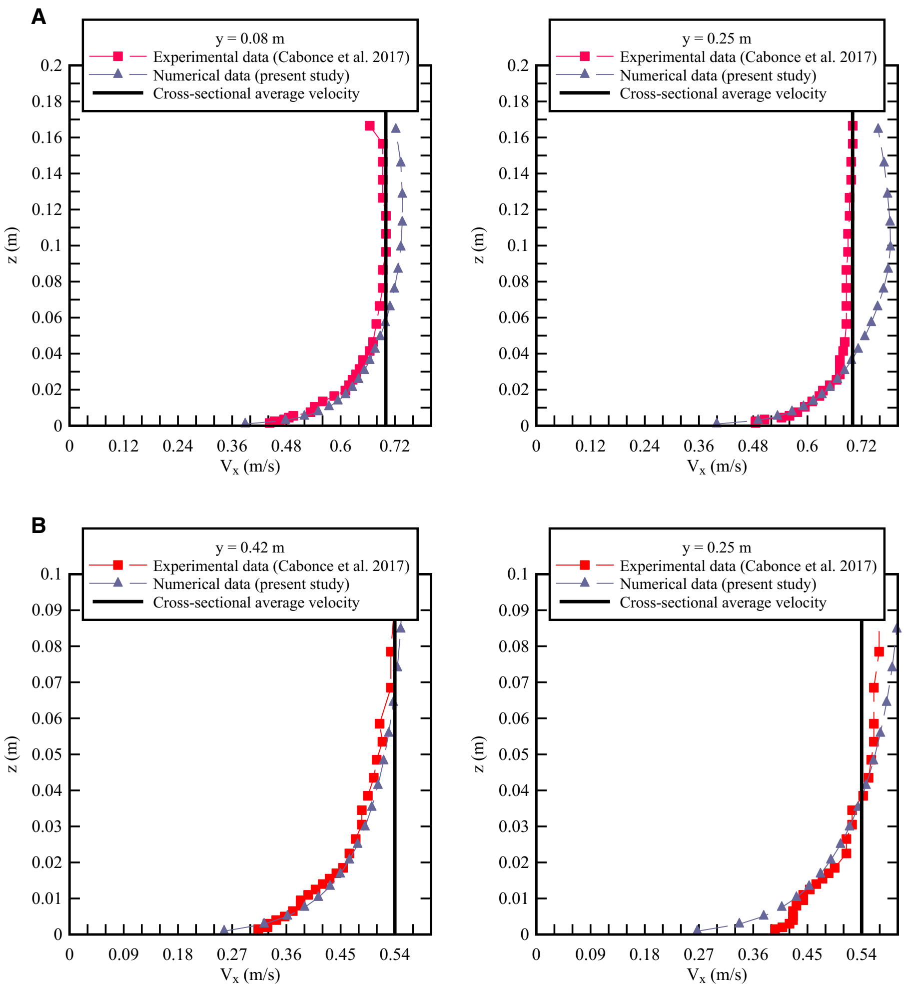

Fig. 5 Longitudinal velocity distribution in a box culvert barrel: comparison between cross-sectional averaged velocity, CFD numerical and physical data; experiments by Cabonce et al. [7]; Left: all measurements near the sidewalls (0.08 m from sidewall); Right: measurements on the channel centreline (y = 0.25 m). **a** Q = 0.056 m^3/s, f = 0.0162. **b** Q = 0.026 m^3/s, f = 0.0145

nature of the culvert design (different targeted flood events for different regional councils), it is unrealistic to conduct CFD modelling for all possible design scenarios. Further, not all local governments and engineering companies have the capacity to conduct detailed numerical CFD modelling. The calculation for percentage of flow area of low velocity zones must be generalised, with self-defined criteria for low velocity, independently of the hydrology requirement, i.e. whether the targeted storm event is about 1:5 ARI or 1:1 ARI. Thus the present study examined the relationship between local fluid velocity V and the associated flow area where the local velocity is less than a characteristic fish swimming speed, e.g. set by a regulatory agency or based upon biological observations and swimming test data. All compiled data are presented in a

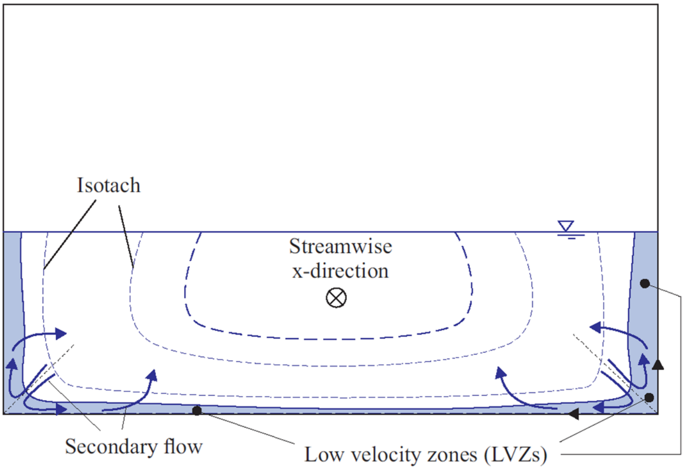

Fig. 6 Definition sketch of low velocity zones in a box culvert barrel, looking downstream

dimensionless form in Fig. 7, for a channel aspect ratio within $1 < B_{cell}/d < 9$. Details of flow conditions for data in Fig. 7 are regrouped in Table 1.

All cases showed a similar trend, with quantitatively close results, albeit some scatter (Fig. 7). The results showed a monotonic increase in relative LVZ area with increasing characteristic swim speed V. In Fig. 7, the solid black curve represents the best-fit correlation of all datasets, whereas the two dashed lines illustrate the upper and lower bounds of the scatter. For an area fraction of 15%, the maximum difference between the two bounds of the data scatter was approximately 10%. The quantitative differences between datasets seemed to show little effect to the aspect ratio B/d. The present CFD results are compared to past CFD and experimental works in Fig. 8, encompassing data with a channel aspect ratio $0.6 < B/d < 13$. The data are further compared to an analytical solution for a two-dimensional turbulent flow, assuming a velocity distribution with a 1/N-th power law:

$$A = \left(\frac{N}{N+1}\right)^N \left(\frac{V}{V_{mean}}\right)^N \tag{21}$$

with A the percentage of flow area ($0 < A < 1$), V_{mean} the bulk velocity, and (V/V_{mean}) is the relative targetted fish swimming speed. Equation (21) is plotted for $N = 4.5$ in Fig. 8. The present CFD results showed a close agreement with past CFD data, albeit these were limited to only a few data points. The experimental data showed overall a larger LVZ area fractions for the same relative velocity compared to the CFD data. The lower bound of experimental data agreed closely with the upper bound of CFD data scatter.

It is worth to note a few advantages of using such a dimensionless plot (Fig. 8). First the plot is independent of hydrological implication, which could vary upon requirement of different councils and sites. Second the results are independent of the barrel culvert cell size, aspect ratio of the barrel flow and downstream tailwater conditions.

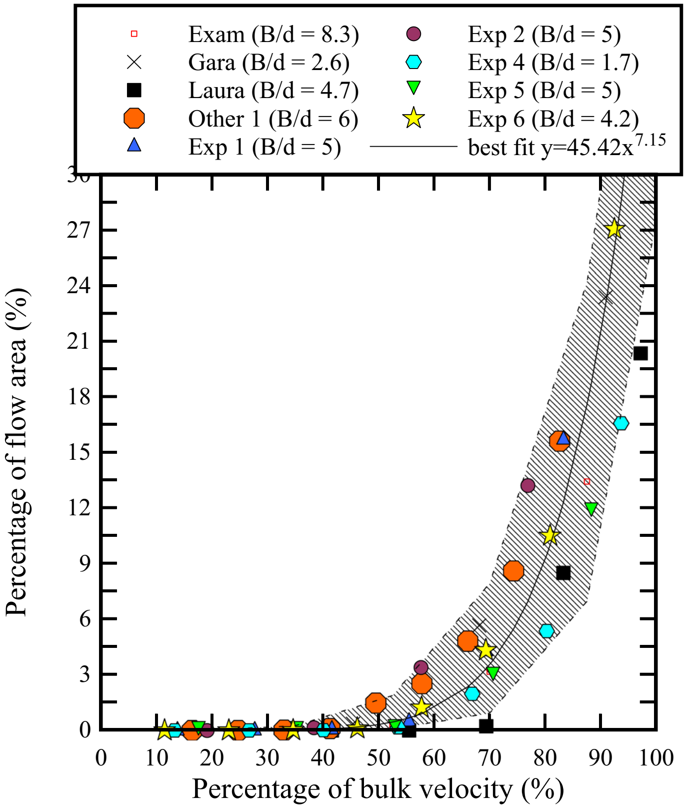

Fig. 7 Dimensionless area fraction of flow less than a relative longitudinal velocity V/V_{mean} (percentage of bulk velocity) where V_{mean} is the bulk velocity, i.e. cross-sectional mean velocity in the barrel—all cases compiled with an aspect ratio within $1 < B_{cell}/d < 9$

5 Hybrid modelling: a discussion

The present study used hybrid modelling, i.e. a combination of physical and CFD modelling, to investigate low velocity zones in a standard box culvert barrel. Both physical measurements and numerical CFD models were employed with support of 1D theoretical solutions, and systematic validations were performed across data sets. The hybrid modelling approach gave a high level of confidence for all data sets through cross-comparison and detailed validation. It encompassed a much wider range of flow conditions, geometric configurations and tailwater conditions. However, the cost of conducting hybrid modelling, especially using full-scale large laboratory facilities and advanced CFD algorithms, is far from trivial. Such research requires expensive equipment, including a relatively large size flume or culvert model and a velocimeter with high-temporal resolution and three-dimensional velocity-sampling head. The process of conducting numerical research, CFD in particular, is demanding in computational power and can be costly, when a commercial CFD program is used. In addition, hybrid modelling requires dual expertise in the fields of physical and numerical modelling: i.e., a fundamental understanding of the numerical model and its limitations, in addition to an in-depth knowledge of the physical model, its

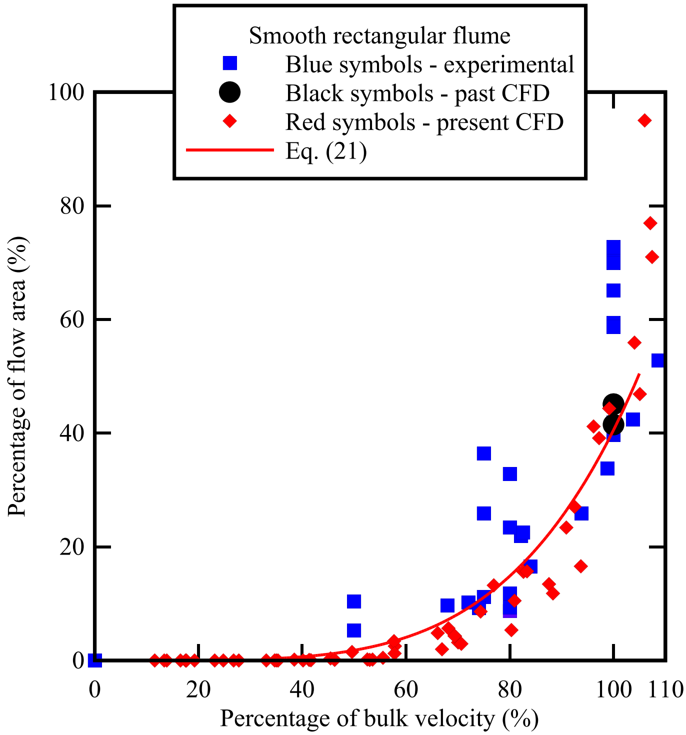

Fig. 8 Dimensionless area fraction of flow less than a relative longitudinal velocity V/V_{mean}, where V_{mean} is the bulk velocity, i.e. cross-sectional mean velocity in the barrel—all cases compared to past CFD [25], experimental studies [7, 24, 26, 27, 34], and Equation (16) assuming $N = 4.5$—rectangular channels with an aspect ratio within $0.6 < B/d < 13$

characteristics, and its instrumentation [23]. Although experimental expertise is critical to a successful CFD validation, it is important to stress that not all experimental setups are truly equal, and both numerical and physical models are developed to reproduce a complicated 3D turbulent flow in a prototype structure.

Altogether, hybrid modelling must be considered an optimum technique in modern engineering designs, by delivering high quality and physically meaningful data set. The technically-challenging nature and high cost are the main issues and such researches are still rare. The current study offers some insight on the capacity of hybrid modelling in hydraulic and mechanical engineering practice.

6 Conclusion

As an open channel, a culvert is designed to stream flows under an embankment. The culvert barrel is the throat of a standard-box culvert with constant width. Current engineering practices emphasise the culvert's capacity to pass flood water at a minimum cost, leading to excessive velocities inside barrel, creating barriers for small-body-mass fish to migrate upstream. Since many physical observations showed fish swimming upstream along the culvert barrel's sidewalls and bottom corners, the present study investigated the velocity field in a standard box culvert barrel, to characterise accurately the low velocity zones (LVZs) in which fish swim and migrate. The work used a hybrid modelling technique, composed of physical measurements, numerical CFD model and 1D theoretical calculations.

The CFD models showed a good capacity in predicting the three-dimensional flow field in the culvert barrel, where the local velocity field was calculated and the low velocity zones were quantified. The systematic validation against physical data is uppermost critical to ascertain the performances of a numerical model. By conducting CFD modelling over a wide range of flow conditions and box cell configurations, a physically-based relationship was derived from numerical and experimental data of past and present studies, correlating the dimensionless flow area with a normalised local velocity V/V_{mean}. Namely, the results showed a monotonic increase in relative LVZ area with increasing characteristic fish swimming speed, irrespective of the aspect ratio B/d and tailwater conditions.

Acknowledgements The authors thank Dr Matthew GORDOS and Marcus RICHES (NSW DPI Fisheries, Australia), and Professor Colin J. APELT (The University of Queensland, Australia) for very helpful discussions. The authors further acknowledge the assistance of Ms Matilda MEPPEM and Mr Tianwei YIN (The University of Queensland, Australia) in conducting a number of tests using CFD models. The financial support of Australian Research Council (Grant LP140100225) and Queensland Department of Transport and Main Roads (TMTHF1805) is acknowledged.

Compliance with ethical standards

Conflict of interest Hubert CHANSON has competing interest and conflict of interest with Craig E. FRANKLIN.

References

1. ANSYS® Academic Research, Release 18.0 (2017) Help System, ANSYS Fluent User's Guide, ANSYS, Inc
2. Apelt CJ (1983) Hydraulics of minimum energy culverts and bridge waterways. Aust Civ Eng Trans CE25(2):89–95
3. Behlke CE, Kane DL, McLeen RF, Travis MT (1991) Fundamentals of culvert design for passage of weak-swimming fish. Report FHW A-AK-RD-90-10. Department of Transportation and Public Facilities, State of Alaska, Fairbanks, USA
4. Blank MD (2008) Advanced studies of fish passage through culverts: 1-D and 3-D hydraulic modelling of velocity, fish energy expenditure, and a new barrier assessment method. Ph.D. thesis, Montana State University, Department of Civil Engineering
5. Boussinesq J (1897) Essai sur la théorie des eaux courantes. Mémoires présentés par divers savants à l'Académie des Sciences 23(1):1–680 **(in French)**
6. British Standard (1943) Flow measurement. British Standard Code BS 1042:1943, British Standard Institution, London
7. Cabonce J, Fernando R, Wang H, Chanson H (2017) Using triangular baffles to facilitate upstream fish passage in box culverts: physical modelling. Hydraulic model Report No. CH107/17. School of Civil Engineering, The University of Queensland, Brisbane, Australia
8. Cabonce J, Wang H, Chanson H (2018) Ventilated corner baffles to assist upstream passage of small-bodied fish in box culverts. J Irrig Drain Eng ASCE 144(8):0418020. https://doi.org/10.1061/(asce)ir.1943-4774.0001329
9. Cabonce J, Fernando R, Wang H, Chanson H (2019) Using small triangular baffles to facilitate upstream fish passage in standard box culverts. Environ Fluid Mech 19(1):157–179. https://doi.org/10.1007/s10652-018-9604-x
10. Chanson H (2000) Introducing originality and innovation in engineering teaching: the hydraulic design of culverts. Eur J Eng Educ 25(4):377–391. https://doi.org/10.1080/03043790050200421
11. Chanson H (2004) The hydraulics of open channel flow: an introduction, 2nd edn. Butterworth-Heinemann, Oxford

12. Chanson H, Leng X (2018) On the development of hydraulic engineering guidelines for fish-friendly standard box culverts, with a focus on small-body fish. Civil Engineering Research Bulletin No. 25, School of Civil Engineering, The University of Queensland, Brisbane, Australia
13. Fairfull S, Witheridge G (2003) Why do fish need to cross the road? Fish passage requirements for waterway crossings. NSW Fisheries, Cronulla, NSW, Australia
14. Hee M (1969) Hydraulics of culvert design including constant energy concept. In: Proceedings of the 20th conference of local authority engineers. Department of Local Government, Queensland, Australia, paper 9, pp 1–27
15. Henderson FM (1966) Open channel flow. MacMillan Company, New York
16. Herr LA, Bossy HG (1965) Hydraulic charts for the selection of highway culverts. Hydraulic Engineering Circular, US Department of Transportation, Federal Highway Administration, HEC No. 5
17. Hirt C, Nichols B (1981) Volume of fluid (VOF) method for the dynamics of free boundaries. J Comput Phys 39(1):201–225
18. Jensen KM (2014) Velocity reduction factors in near boundary flow and the effect on fish passage through culverts. Master of Science thesis, Brigham Young University, USA
19. Khodier MA, Tullis BP (2014) Fish passage behavior for severe hydraulic conditions in baffled culverts. J Hydraul Eng ASCE 140(3):322–327. https://doi.org/10.1061/(ASCE)HY.1943-7900.0000831
20. Larinier M (2002) Fish passage through culverts, rock weirs and estuarine obstructions. Bulletin Français de Pêche et Pisciculture 364:119–134
21. Launder BE, Spalding DB (1974) The numerical computation of turbulent flows. Comput Methods Appl Mech Eng 3(2):269–289
22. Leng X, Chanson H (2018) Modelling low velocity zones in box culverts to assist fish passage. In: Lau TCW, Kelso RM (eds) Proceedings of 21st Australasian fluid mechanics conference, Adelaide, Australia, 10–13 December, p 547
23. Leng X, Simon B, Khezri N, Lubin P, Chanson H (2019) CFD modelling of tidal bores: development and validation challenges. Coast Eng J. https://doi.org/10.1080/21664250.2018.1498211
24. Macintosh JC (1990) Hydraulic characteristics in channels of complex cross-section. Ph.D. thesis, School of Civil Engineering, The University of Queensland, Brisbane, Australia
25. Naot D, Rodi W (1982) Numerical simulations of secondary currents in channel flow. J Hydraul Div ASCE 108(HY8):948–968
26. Nezu I, Rodi W (1985) Experimental study on secondary currents in open channel flow. In: Proceedings of the 21st IAHR Congress, IAHR, Melbourne, pp 115–119
27. Nikuradse J (1926) Untersuchungen über die geschwindigkeitsverteilung in turbulenten strömungen. Ph.D. thesis, Gottingen, VDI Forsch
28. Olsen A, Tullis B (2013) Laboratory study of fish passage and discharge capacity in slip-lined, baffled culverts. J Hydraul Eng ASCE 139(4):424–432
29. Quadrio J (2007) Passage of fish through drainage structures. Qld Roads (4):6–17
30. Roache PJ (1998) Fundamentals of computational fluid dynamics. Hermosa Publishers
31. Wang H, Chanson H (2018) Modelling upstream fish passage in standard box culverts: interplay between turbulence, fish kinematics, and energetics. River Res Appl 34(3):244–252. https://doi.org/10.1002/rra.3245
32. Wang H, Chanson H, Kern P, Franklin C (2016) Culvert hydrodynamics to enhance upstream fish passage: fish response to turbulence. In: Ivey G, Zhou T, Jones N, Draper S (eds) Proceedings of 20th Australasian Fluid Mechanics Conference, Australasian Fluid Mechanics Society, Perth, WA, Australia, 5–8 December, p 682. ISBN 978 2 74052 377 6
33. Warren ML Jr, Pardew MG (1998) Road crossings as barriers to small-stream fish movement. Trans Am Fish Soc 127:637–644
34. Xie Q (1998) Turbulent flows in non-uniform open channels: experimental measurements and numerical modelling. Ph.D. thesis, School of Civil Engineering, The University of Queensland, Brisbane, Australia
35. Zhang G, Chanson H (2018) Three-dimensional numerical simulations of smooth, asymmetrically roughened, and baffled culverts for upstream passage of small-bodied fish. River Res Appl 34(8):957–964. https://doi.org/10.1002/rra.3346